STD and WLOGSY NMR Based Fingerprinting Reveals Subtle and Biologically Relevant Differences in Short Linear Motif Binding

Marwaan Rylands,*[1] Daniel A. Kusza,[1] David J. Clarke,[2] Beatriz G. de la Torre,[3] Fernando Albericio,[4] Adrienne L. Edkins,[5] and Clinton G.L. Veale*[1]

[1]Department of Chemistry, University of Cape Town, Rondebosch, Cape Town, 7701, South Africa.

[2]EaStCHEM, School of Chemistry, University of Edinburgh, Joseph Black Building, David Brewster Road, Edinburgh, EH93FJ

[3]School of Laboratory Medicine and Medical Sciences, University of Kwa-Zulu Natal, 4001, South Africa

[4]School of Chemistry and Physics, University of Kwa-Zulu Natal, Westville, 4041, South Africa

[5]Biomedical Biotechnology Research Unit (BioBRU), Department of Biochemistry and Microbiology, Rhodes University, Makhanda, 6139, South Africa.

*Correspondence: marwaan.rylands@uct.ac.za, clinton.veale@uct.ac.za

Abstract: Interactions between Short Linear Motifs (SLiMs) and a partner domain are commonly exploited as simplified functional models of transient Protein-Protein Interactions (PPI) for characterizing interfacial associations between partner proteins. In this study, we report the use of a ligand-observed NMR approach, where through unambiguous assignment of ^{1}H resonances of two closely related SLiMs, whilst bound to their partner domain (Hop$_{TPR2A}$), we could assign STD and WLOGSY NMR signals to specific regions in the peptide backbone. These data revealed subtle alterations in magnetization transfer, resulting from changes in the binding mode of each SLiM respectively. The ability to detect and compare these changes at sub-residue resolution, provided differing fingerprints of SLiM binding. This approach therefore represents a broadly accessible method for identifying binding hot spots and interrogating the impact of structural variations on SLiM-domain interaction stability, and by extension transient PPIs.

Introduction

Transient protein-protein interactions (PPIs), play a central role as mediators of biological pathways, cell metabolism and signaling networks. Minor alterations in the interfacial interactions of PPIs, whether they occur from sequence mutation, or small molecule modulation can have considerable biological consequences.[1–3] Therefore transient PPIs are not only considered a promising class of increasingly druggable targets, but also offer the opportunity to unravel new insight into disease onset and progression.[4–7] The necessity for transient PPIs to be weak or short-lived in duration means that they are typically mediated by the relatively low surface area interactions between a domain from one partner protein and a disordered short linear motif (SLiM) from the corresponding partner.[8–11] This feature of transient PPIs also means that simplified SLiM-domain interactions can operate as competent proxies of the PPI interface, which in turn can be exploited to characterize interfacial information and identify PPI modulatory compounds. To that end numerous biophysical approaches including x-ray crystallography, cryo-electron microscopy (EM) native mass spectrometry (MS), in silico approaches and nuclear magnetic resonance (NMR) have been utilized to study SLiM-domain interactions.[12–17]

Each of these techniques possess an inherent blend of capabilities and limitations with respect to experimental complexity, speed and biological relevance of experimental conditions. Therefore, robust interrogation of SLiM-domain interaction systems and its application to chemical biology and drug discovery requires an array of orthogonal biophysical techniques.[18] Ligand-observed NMR refers to a class of label- free NMR experiments, used to assess the dominant solution-phase conformation of a protein-ligand interaction.[19] Saturation Transfer Difference (STD) and Water Ligand Observed via Gradient Spectroscopy (WLOGSY) NMR, which both exploit the nuclear Overhauser effect (NOE) have found particular utility for probing non-covalent target-ligand interactions.[20] However, while not generally considered useful for gathering protein-observed binding site information, these orthogonal techniques for NMR radio-frequency saturation, can provide significant information pertaining to bound ligand interactions, including identification of strongly interacting regions of a ligand, water accessibility following binding and insight into mechanisms of association.[21–23]

In the context of SLiM-domain interactions as PPI proxies, a set of unambiguously assigned ^{1}H NMR SLiM signals would render STD and WLOGSY NMR data as a high-resolution fingerprint of SLiM binding. Furthermore, binding disparities resulting from domain and/or SLiM sequence changes could be detected through subtle alterations in magnetization transfer and reflected in

the SLiM fingerprint. This would in turn provide valuable interfacial insight, including the impact of domain or SLiM alteration on PPI stability. However, despite its potential, there remain very few examples of ligand-observed NMR being leveraged for these purposes. This is partly due the inherent complexity of peptide NMR spectra, and the signal overlap amongst α and β proton signals, which complicate elucidations.[24] Furthermore, the potential for chemical shift alterations upon SLiM-domain interaction makes the unambiguous assignment of SLiM ¹H signals or the purposes of STD and WLOGSY fingerprinting, non-trivial.

The SLiM-domain interaction between the Hsp90 C-terminal (Hsp90$_{CTD}$) MEEVD pentapeptide and the TPR2A domain of Hop (Hop$_{TPR2A}$, **Figure 1A**) is a well-characterized proxy of the full-length Hop-Hsp90 PPI.[25,26] Through a series of studies, we have shown that while an acetylated analogue of the interfacial SLiM (**1, Figure 1B**) has no PPI modulatory activity, a closely related, tetrazole-containing analogue (**2**) was capable of PPI inhibition, by competing for MEEVD binding.[27–29] This observation suggests that despite their structural homology, these peptides differ in their engagement with Hop$_{TPR2A}$, although a structural explanation of this phenomenon is lacking. Accordingly, in this study, we report a resource-efficient ligand-observed NMR approach which allowed us to discern subtle alterations between the interactions of the closely related peptides with Hop$_{TPR2A}$, including identification of hot spots on the SLiM, which will inform future design of PPI modulators. This fingerprinting approach is not only specifically applicable to the Hop-Hsp90 interface but has broader applications as accessible tool for structural interrogation of SLiM- mediated transient PPIs.

Results and Discussion

For the purposes of assigning ¹H resonances, we numbered each relevant proton according to **Figure 1B.** Beginning with a spectral analysis of the Hop$_{TPR2A}$ – **1** complex (**Figure 2, Table S1**), TOCSY NMR was particularly useful for assigning the proton network within an amino acid residue, while NOESY NMR allowed for amido *NH* resonances to be assigned via through space correlation to the α-proton of the neighbouring amino acid. Our assignment origin was the V4 residue, where the isopropyl methyl signals (H-16, δ 0.78) were clearly distinguishable. This then allowed us to assign the V4 amido *NH* (H-13, δ8.05) and α-protons (H-14, δ4.11), respectively. NOESY correlations between H-14 and the D5 amido *NH* (H-17, δ7.87), and H-13 and the E3 α-proton (H-12, δ4.30) allowed assignment of both residues, which in turn, facilitated the

assignment of the D5 α-protons (H-18, δ4.24), the diastereotopic D5 methylene protons H-19 and H-20 (δ 2.45, 2.55) and the E3 amido *NH* (H-11, δ8.31) through TOCSY cross peaks.

Through this approach, we were further, able to assign the E2 α-proton (H-8, δ4.21), alongside the outstanding M1 residues, including the M1 *NH* (H-2, δ8.21), α- (H-3, δ4.33), *S*-methyl (H-6, δ 1.90) and terminal acetyl (H-1, δ 1.98). However, the corresponding β (H-9) and γ (H-10) positions on the E2 and E3 side chains were indistinguishable and were assigned the same residue number (**Table S1, Figure 1B**). We subsequently applied this template to peptide **2**, where again, we successfully distinguished proton resonances apart from the corresponding β and γ positions on the E2 and Tr3 side chains, which were again assigned the same number.

We proceeded to fingerprinting peptide binding through STD and WLOGSY NMR. In recording STD NMR data, two separate experiments are acquired. The first, (on-resonance) spectrum, applies selective radio frequencies to the protein where magnetization is transferred from the protein to the bound ligand via NOE and the second (off-resonance) spectrum is acquired without the selective irradiation of the protein. Subtracting the signal intensity of the off-resonance spectrum signals, from that observed in-resonance spectrum results in the STD spectrum, where only, signals magnetized via the NOE effect remain. Relative quantification of STD efficiency, (determined as a percent of the largest STD signal) is indicative of relative proximity to the protein surface (**Figure 3** and **4**). Analysis of the STD NMR the Hop$_{TPR2A}$ – **1** complex showed that all identifiable proton resonances were in sufficient proximity to the protein to undergo magnetization via NOE. This suggested that all these regions contributed in some fashion to the binding of peptide **1**. The mean STD intensity was calculated as 23% per resonance, and this value was used as a lower limit, for characterizing significant binding contributions (**Figure 4** and **Table S1**). STD intensity was the most pronounced for the E2 α-proton (H-8, 100%) indicating a particularly close contact. The signal intensities of the α-protons of V4 (H-14, 35%), M1 (H-3, 25%), E3 α-proton (H-12, 23%) and the D5 *NH* (H-17, 26%) all equalled or exceeded the mean intensity (23%) and were considered comparatively important interacting regions (**Figure 4, Table S1**). Similarly, all identifiable proton resonances in the Hop$_{TPR2A}$ – **2** complex showed STD NMR signals, also with a mean intensity of 23%. The E2 α-proton signal was again found to have a relative intensity of 100%, while the V4 (43%) and M1 (37%), were also identified as prominent interacting regions. While in comparison to the Hop$_{TPR2A}$ – **1** complex, the relative intensity of the D5 *NH*, was substantially reduced (10%) the D5 α-proton signal (H-18, 37%), emerged as a significant relative contributor, indicating, a slight alteration in binding conformation at the D5 residue. The most significant change in the STD spectral data between the complexes of **1** and **2**

with Hop$_{TPR2A}$ was observed for the Tr3 α-proton (H-12, 100%) whose relative signal intensity was equal to H-8 (**Figure 4**). This shift indicated a substantial alteration in protein proximity, resulting from the tetrazole bioisosteric replacement. Despite these alterations, the STD intensities of unassigned E2/E3 and E2/Tr3 residues H-9 and H-10 were both lower than their respective means and were considered to be making comparatively negligible contributions to binding.

We then proceeded to conduct a WLOGSY analysis of both complexes. During WLOGSY acquisitions, polarization is transferred from water molecules to bound ligands by NOE. An NOE transfer from protein-bound water will lead to signal suppression or inversion (-ve WLOGSY), while interaction with bulk water, will not be inverted (+ve WLOGSY).[30] Quantification of this effect provides insight into the relative strength of interaction of specific regions of a bound-ligand via its interaction with protein-bound waters. With respect to the Hop$_{TPR2A}$ – **1** complex, all peptide signals were either supressed or inverted (**Figure 5A**). The most pronounced WLOGSY inversions were observed for the amido *NH*'s of M1 (-87%) and E2 (-100%) followed by a slight reduction in intensity for the E3 *NH* (-76%), and a more substantial reduction for the V4 *NH* (-14%) (**Figure 6**). While the signal was suppressed, no inversion was observed for the D5 *NH*. In addition, a substantial WLOGSY inversion was observed for the M1 methyl (H-6, -52%), while a moderate inversion was observed for the valine methyl signals (H-16, -26%). One additional weak WLOGSY inversion was observed for the *N*-acetamide (H-1, -14%). With respect to the Hop$_{TPR2A}$ – **2** complex, the patterns of the WLOGSY inversions of the amido *NH*'s mirrored that of Hop$_{TPR2A}$ – **1**. However, the relative magnitude of the signals was generally enhanced, including at the Tr3 (-95%) and V4 *NH*s (-28%) respectively (**Figure 6**). Interestingly, the H-1, H -6, and H-14 nuclei appeared as +ve WLOGSY signals (**Figures 5** and **6**), suggesting that these nuclei were experiencing reduced NOE transfer from bound waters. This contrast to the corresponding signals emanating from the Hop$_{TPR2A}$ – **1** complex are likely as a result of altered binding conformation at this residue.

Conclusion

By conducting 2-dimensional proton correlation spectroscopy (TOCSY and NOESY) on synthetic MEEVD analogues (**1** and **2**) whilst individually bound to Hop$_{TPR2A}$, we were able to confidently assign most of the resonances of both peptides in an experimentally relevant context, which in turn allowed for effective interpretation of STD and WLOGSY NMR data. While this approach was unable to deduce the specific impact of acidic residues,[31] we could discern subtle alterations in the interactions between the closely related peptides with Hop$_{TPR2A}$. This included highlighting the

significant contribution made to binding by the E2 residue in both peptides. This observation was in close agreement, with reported SAR information, which suggested that the E2 residue was essential for PPI inhibitory activity.[29] Bioisosteric replacement of E3 with Tr3 residue resulted in a noticeable increase in the interactions with Hop$_{TPR2A}$.

Whilst to some extent, this may explain the vastly different PPI modulatory activity between peptides **1** and **2**,[27] this alteration also precipitated alterations in patterns of NOE transfer, and thus the SLiM observed NMR 'fingerprint' (**Figure 7**). Together, these data points toward differences in target engagement at these residues, which will likely impact biological activity. The ability to identify ligand regions whose interactions are seemingly less critical for binding, and thus targeted for removal, or replacement, has useful medicinal chemistry applications. However, possibly more significantly, in the context of transient PPIs, NMR fingerprinting can help identify hot spot resides within the interfacial SLiM at the interface, as well as being applied to ascertain the impact of structural variations on SLiM-domain stability.

Experimental Section

Hop$_{TPR2A}$ and synthetic peptides were produced usign previously reported methodolgy.[27] For NMR studies, protein samples were buffer exchanged into 50 mM Na$_2$HPO$_4$ buffer using a Zeba Spin Desalting Column (Thermo Fisher Scientific) underwent buffer excahnge the peptides and protein were dissolved in 540 µL of buffer (50 mM KH$_2$PO$_4$, 50 mM Na$_2$HPO$_4$, pH 7.5, 150 mM NaCl) and 60 µL of H$_2$O. All the spectra were acquired with a Bruker Avance III 600 MHz NMR spectrometer (Bruker Biospin, Rheinstetten, Germany) equipped with a BBO Prodigy cryoprobe and processed using Bruker processing software (Topspin 4.2.0). The 1D ^{1}H and water suppression presaturation experiments were obtained using standard Bruker pulse sequences (zg30 and zgpr). The probe temperature was maintained at 298 K for the duration of the experiments. All 1D ^{1}H spectra were obtained with 64 scans (NS) and prior 8 dummy scans (DS). A relaxation delay (D1) of 1 sec and pulse (P1) of 12 µsec were also used. Water suppression spectra were obtained with an offset (O1) of 2820.47 Hz and all reference ^{1}H spectra were acquired with a sweep width of 19.99 ppm. STD and WLOGSY NMR experiments were acquired using optimised Bruker pulse sequences with water suppression using excitation sculpting (stddifesgp and ephogsygpno.2). STD experiments were acquired at a frequency of -1.0 ppm for on-resonance acquisitions, and 30 ppm for off-resonance acquisitions. The power for the on-resonance saturation pulse (p42) was set between 1x10^{-4} W (40 dB) and 1x10^{-6} W (60 dB). The

spin lock time (D29) was set to 10 ms and the saturation time (D20) was varied between 0.25 and 5 s for STD amplification build-up and optimised D20 determination. The relaxation delay (D1) used for the STD experiments was 15 s and was calculated from T_1, determined from the inversion recovery experiment using the standard Bruker pulse sequence (t1ir). The number of scans (NS) for the STD experiment were also 64, with the number of dummy scans (DS) set to 8. All STD experiments were acquired with interleaved acquisition, with a loop counter (L4) of 4. The STD amplification factor for each unique signal was calculated as the percentage of signal to noise ratio (S/N) in the on-resonance spectra over the signal to noise ratio of the STD spectra. WLOGSY Spectra were acquired with 124 scans. WLOGSY NMR experiments employed a 20 ms selective Gaussian 180° pulse at the water signal frequency (2820.47 Hz) and a NOE mixing time of 1 s. Both STD and WLOGSY spectra were phase and baseline corrected using the automatic baseline and phase correction functions in Topspin 4.2.0. To maximize the S/N ratio of the STD and WLOGSY experiments, a peptide concentration of 2.0 mM and a TPR2A concentration of 40 μM were chosen. ^{1}H NMR chemical shift assignments for the peptides, Ac-MEEVD-OH and Ac-METrVD-OH were achieved via the standard systematic application of 2D COSY, TOCSY, and NOESY experiments.

Supporting Information

Supporting information can be found in the online version of this manuscript.

Acknowledgements

References

(1)   Jubb, H. C.; Pandurangan, A. P.; Turner, M. A.; Ochoa-Montaño, B.; Blundell, T. L.; Ascher, D. B. Mutations at Protein-Protein Interfaces: Small Changes over Big Surfaces Have Large Impacts on Human Health. *Progress in Biophysics and Molecular Biology*. 2017, pp 3–13. https://doi.org/10.1016/j.pbiomolbio.2016.10.002.

(2)   Cheng, F.; Zhao, J.; Wang, Y.; Lu, W.; Liu, Z.; Zhou, Y.; Martin, W. R.; Wang, R.; Huang, J.; Hao, T.; Yue, H.; Ma, J.; Hou, Y.; Castrillon, J. A.; Fang, J.; Lathia, J. D.; Keri, R. A.; Lightstone, F. C.; Antman, E. M.; Rabadan, R.; Hill, D. E.; Eng, C.; Vidal, M.; Loscalzo, J. Comprehensive Characterization of Protein–Protein Interactions Perturbed by Disease Mutations. *Nat. Genet.* **2021**, *53* (3), 342–353. https://doi.org/10.1038/s41588-020-00774-y.

(3)   Zhong, M.; Lee, G. M.; Sijbesma, E.; Ottmann, C.; Arkin, M. R. Modulating Protein–Protein Interaction Networks in Protein Homeostasis. *Current Opinion in Chemical Biology*. 2019, pp 55–65. https://doi.org/10.1016/j.cbpa.2019.02.012.

(4)   La, D.; Kong, M.; Hoffman, W.; Choi, Y. I.; Kihara, D. Predicting Permanent and Transient Protein-Protein Interfaces. *Proteins Struct. Funct. Bioinforma.* **2013**, *81* (5), 805–818. https://doi.org/10.1002/prot.24235.

(5)   Lu, H.; Zhou, Q.; He, J.; Jiang, Z.; Peng, C.; Tong, R.; Shi, J. Recent Advances in the Development of Protein–Protein Interactions Modulators: Mechanisms and Clinical Trials. *Signal Transduct. Target. Ther.* **2020**, *5* (1), 213. https://doi.org/10.1038/s41392-020-00315-3.

(6)   De Keersmaecker, H.; Camacho, R.; Rantasa, D. M.; Fron, E.; Ujii, H.; Mizuno, H.; Rocha, S. Mapping Transient Protein Interactions at the Nanoscale in Living Mammalian Cells. *ACS Nano* **2018**, *12* (10), 9842–9854. https://doi.org/10.1021/acsnano.8b01227.

(7)   Maculins, T.; Garcia-Pardo, J.; Skenderovic, A.; Gebel, J.; Putyrski, M.; Vorobyov, A.; Busse, P.; Varga, G.; Kuzikov, M.; Zaliani, A.; Rahighi, S.; Schaeffer, V.; Parnham, M. J.; Sidhu, S. S.; Ernst, A.; Dötsch, V.; Akutsu, M.; Dikic, I. Discovery of Protein-Protein Interaction Inhibitors by Integrating Protein Engineering and Chemical Screening Platforms. *Cell Chem. Biol.* **2020**, *27* (11), 1441-1451.e7. https://doi.org/10.1016/j.chembiol.2020.07.010.

(8)   Nevola, L.; Giralt, E. Modulating Protein-Protein Interactions: The Potential of Peptides. *Chem. Commun.* **2015**, *51* (16), 3302–3315. https://doi.org/10.1039/c4cc08565e.

(9)   Cunningham, J. M.; Koytiger, G.; Sorger, P. K.; AlQuraishi, M. Biophysical Prediction of Protein–Peptide Interactions and Signaling Networks Using Machine Learning. *Nat. Methods* **2020**, *17* (2), 175–183. https://doi.org/10.1038/s41592-019-0687-1.

(10)   Perkins, J. R.; Diboun, I.; Dessailly, B. H.; Lees, J. G.; Orengo, C. Transient Protein-Protein Interactions: Structural, Functional, and Network Properties. *Structure* **2010**, *18* (10), 1233–1243. https://doi.org/10.1016/j.str.2010.08.007.

(11)   Acuner Ozbabacan, S. E.; Engin, H. B.; Gursoy, A.; Keskin, O. Transient Protein-Protein Interactions. *Protein Eng. Des. Sel.* **2011**, *24* (9), 635–648. https://doi.org/10.1093/protein/gzr025.

(12)   Ballone, A.; Lau, R. A.; Zweipfenning, F. P. A.; Ottmann, C. A New Soaking Procedure for X-Ray Crystallographic Structural Determination of Protein-Peptide Complexes. *Acta Crystallogr. Sect. F Struct. Biol. Commun.* **2020**, *76*, 501–507. https://doi.org/10.1107/S2053230X2001122X.

(13)   Chang, R.; Zhang, X.; Qiao, A.; Dai, A.; Belousoff, M. J.; Tan, Q.; Shao, L.; Zhong, L.; Lin, G.; Liang, Y. L.; Ma, L.; Han, S.; Yang, D.; Danev, R.; Wang, M. W.; Wootten, D.; Wu, B.; Sexton, P. M. Cryo-Electron Microscopy Structure of the Glucagon Receptor with a Dual-Agonist Peptide. *J. Biol. Chem.* **2020**, *295* (28), 9313–9325. https://doi.org/10.1074/jbc.ra120.013793.

(14)   Bellamy-Carter, J.; Mohata, M.; Falcicchio, M.; Basran, J.; Higuchi, Y.; Doveston, R. G.; Leney, A. C. Discovering Protein-Protein Interaction Stabilisers by Native Mass Spectrometry. *Chem. Sci.* **2021**, *12* (32), 10724–10731. https://doi.org/10.1039/d1sc01450a.

(15)   Brancaccio, D.; Di Maro, S.; Cerofolini, L.; Giuntini, S.; Fragai, M.; Luchinat, C.; Tomassi, S.; Limatola, A.; Russomanno, P.; Merlino, F.; Novellino, E.; Carotenuto, A. HOPPI-NMR: Hot-Peptide-Based Screening Assay for Inhibitors of Protein–Protein Interactions by NMR. *ACS Med. Chem. Lett.* **2020**, *11* (5), 1047–1053. https://doi.org/10.1021/acsmedchemlett.9b00620.

(16)   Chang, L.; Perez, A. Ranking Peptide Binders by Affinity with AlphaFold**. *Angew. Chemie - Int. Ed.* **2023**, *62* (7), e202213362. https://doi.org/10.1002/anie.202213362.

(17)   Veale, C. G. L.; Clarke, D. J. Mass Spectrometry-Based Methods for Characterizing Transient Protein–Protein Interactions. *Trends in Chemistry*. 2024, pp 377–391. https://doi.org/10.1016/j.trechm.2024.05.002.

(18)   Renaud, J. P.; Chung, C. W.; Danielson, U. H.; Egner, U.; Hennig, M.; Hubbard, R. E.; Nar, H. Biophysics in Drug Discovery: Impact, Challenges and Opportunities. *Nature Reviews Drug Discovery*. 2016, pp 679–698. https://doi.org/10.1038/nrd.2016.123.

(19)   Becker, W.; Bhattiprolu, K. C.; Gubensäk, N.; Zangger, K. Investigating Protein–Ligand Interactions by Solution Nuclear Magnetic Resonance Spectroscopy. *ChemPhysChem*.

2018, pp 895–906. https://doi.org/10.1002/cphc.201701253.

(20)   Calabrese, D. R.; Connelly, C. M.; Schneekloth, J. S. Ligand-Observed NMR Techniques to Probe RNA-Small Molecule Interactions. *Methods Enzymol.* **2019**, *623*, 131–149. https://doi.org/10.1016/bs.mie.2019.05.030.

(21)   Monaco, S.; Angulo, J.; Wallace, M. Imaging Saturation Transfer Difference (STD) NMR: Affinity and Specificity of Protein-Ligand Interactions from a Single NMR Sample. *J. Am. Chem. Soc.* **2023**, *145* (30), 16391–16397. https://doi.org/10.1021/jacs.3c02218.

(22)   Nepravishta, R.; Walpole, S.; Tailford, L.; Juge, N.; Angulo, J. Deriving Ligand Orientation in Weak Protein–Ligand Complexes by DEEP-STD NMR Spectroscopy in the Absence of Protein Chemical-Shift Assignment. *ChemBioChem* **2019**, *20* (3), 340–344. https://doi.org/10.1002/cbic.201800568.

(23)   Monaco, S.; Tailford, L. E.; Juge, N.; Angulo, J. Differential Epitope Mapping by STD NMR Spectroscopy To Reveal the Nature of Protein–Ligand Contacts. *Angew. Chemie - Int. Ed.* **2017**, *56* (48), 15289–15293. https://doi.org/10.1002/anie.201707682.

(24)   Daniecki` NJ, Costantini NV, Sametz GM, Z. N. A Dataset of Simple 1-D and 2-D NMR Spectra of Peptides, Including All Encoded Amino Acids, for Introductory Instruction in Protein Biomolecular NMR Spectroscopy. *ChemRxiv* **2024**, 10.26434/chemrxiv-2024-zww4n.

(25)   Brinker, A.; Scheufler, C.; Von Der Mülbe, F.; Fleckenstein, B.; Herrmann, C.; Jung, G.; Moarefi, I.; Ulrich Hartl, F. Ligand Discrimination by TPR Domains. Relevance and Selectivity of EEVD-Recognition in Hsp70·Hop·Hsp90 Complexes. *J. Biol. Chem.* **2002**, *277* (22), 19265–19275. https://doi.org/10.1074/jbc.M109002200.

(26)   Scheufler, C.; Brinker, A.; Bourenkov, G.; Pegoraro, S.; Moroder, L.; Bartunik, H.; Hartl, F. U. U.; Moarefi, I. Structure of TPR Domain – Peptide Complexes : Critical Elements in the Assembly of the Hsp70 – Hsp90 Multichaperone Machine. *Cell* **2000**, *101* (2), 199–210. https://doi.org/10.1016/S0092-8674(00)80830-2.

(27)   Veale, C. G. L.; Mateos-Jiménez, M.; Vaaltyn, M. C.; Müller, R.; Makhubu, M. P.; Alhassan, M.; de la Torre, B. G.; Albericio, F.; Mackay, C. L.; Edkins, A. L.; Clarke, D. J. A Native Mass Spectrometry Platform Identifies HOP Inhibitors That Modulate the HSP90–HOP Protein–Protein Interaction. *Chem. Commun.* **2021**, *57,* 10919–10922. https://doi.org/10.1039/d1cc04257b.

(28)   Veale, C. G. L.; Chakraborty, A.; Mhlanga, R.; Albericio, F.; de la Torre, B. G.; Edkins, A. L.; Clarke, D. J. A Native Mass Spectrometry Approach to Qualitatively Elucidate Interfacial Epitopes of Transient Protein-Protein Interactions. *Chem. Commun.* **2024**, *60* (45), 5844–

5847. https://doi.org/10.1039/d4cc01251h.

(29)   Okpara, M. O.; Vaaltyn, M. C.; Watson, J. L.; Alhassan, M.; Albericio, F.; de la Torre, B. G.;
Clarke, D. J.; Veale, C. G. L.; Edkins, A. L. Modulators of the Hop-HSP90 Protein–Protein
Interaction Disrupt KSHV Lytic Replication. *ACS Infect. Dis.* **2024**,
10.1021/acsinfecdis.4c00429. https://doi.org/10.1021/acsinfecdis.4c00429.

(30)   Bataille, C. J. R.; Rabbitts, T. H.; Claridge, T. D. W. NMR WaterLOGSY as An Assay in Drug
Development Programmes for Detecting Protein-Ligand Interactions–NMR WaterLOGSY.
Bio-protocol **2020**, *10* (13), e3666. https://doi.org/10.21769/BioProtoc.3666.

(31)   Albohy, A.; Richards, M. R.; Cairo, C. W. Mapping Substrate Interactions of the Human
Membrane-Associated Neuraminidase, NEU3, Using STD NMR. *Glycobiology* **2014**, *25*
(3), 284–293. https://doi.org/10.1093/glycob/cwu109.
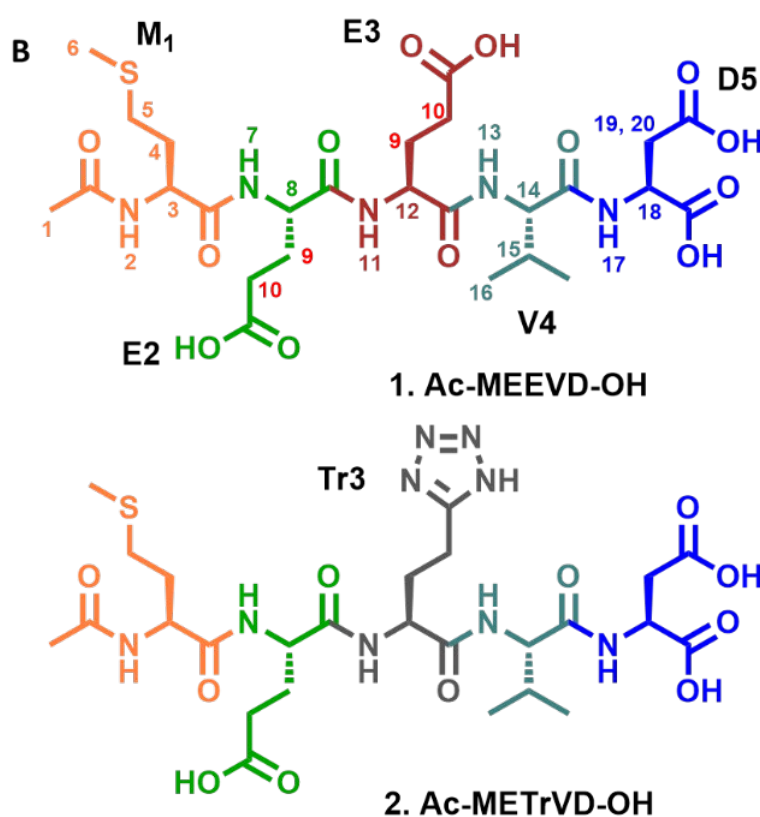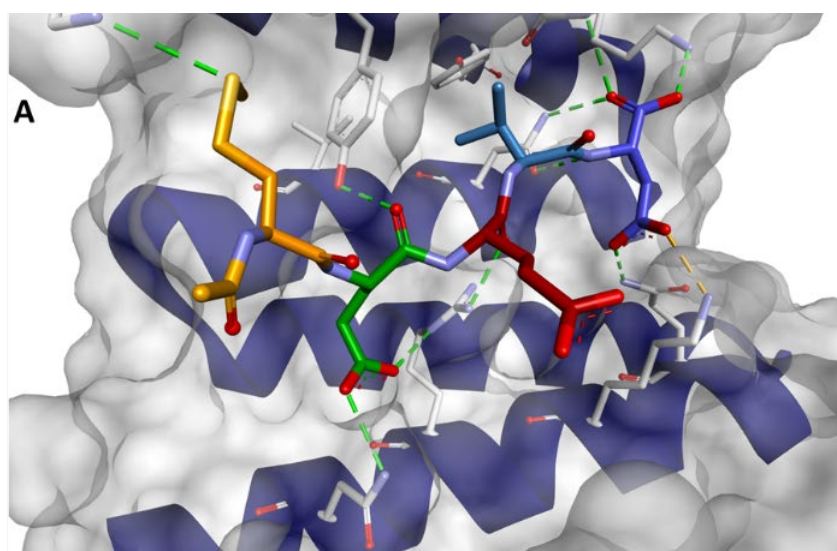
Figure 1. A: X-ray co-crystal structure of acetylated MEEVD-OH (peptide **1**) bund to Hop$_{TPR2A}$. (PDB 1ELR). This SLiM-domain interaction is commonly used as a proxy for the full Hop-Hsp90 PPI. **B**: Peptides used in this study. Peptide **1** is an acetylated analogue of the naturally occurring MEEVD SLiM, which has no PPI inhibitor activity. However, Peptide **2**, is capable of PPI inhibition, suggesting subtle alterations in target engagement. Peptides are coloured per residue to match data shown in **Figures 2, 4** and **6**. Numbering of structures corelates to numbering used for NMR structural elucidation.
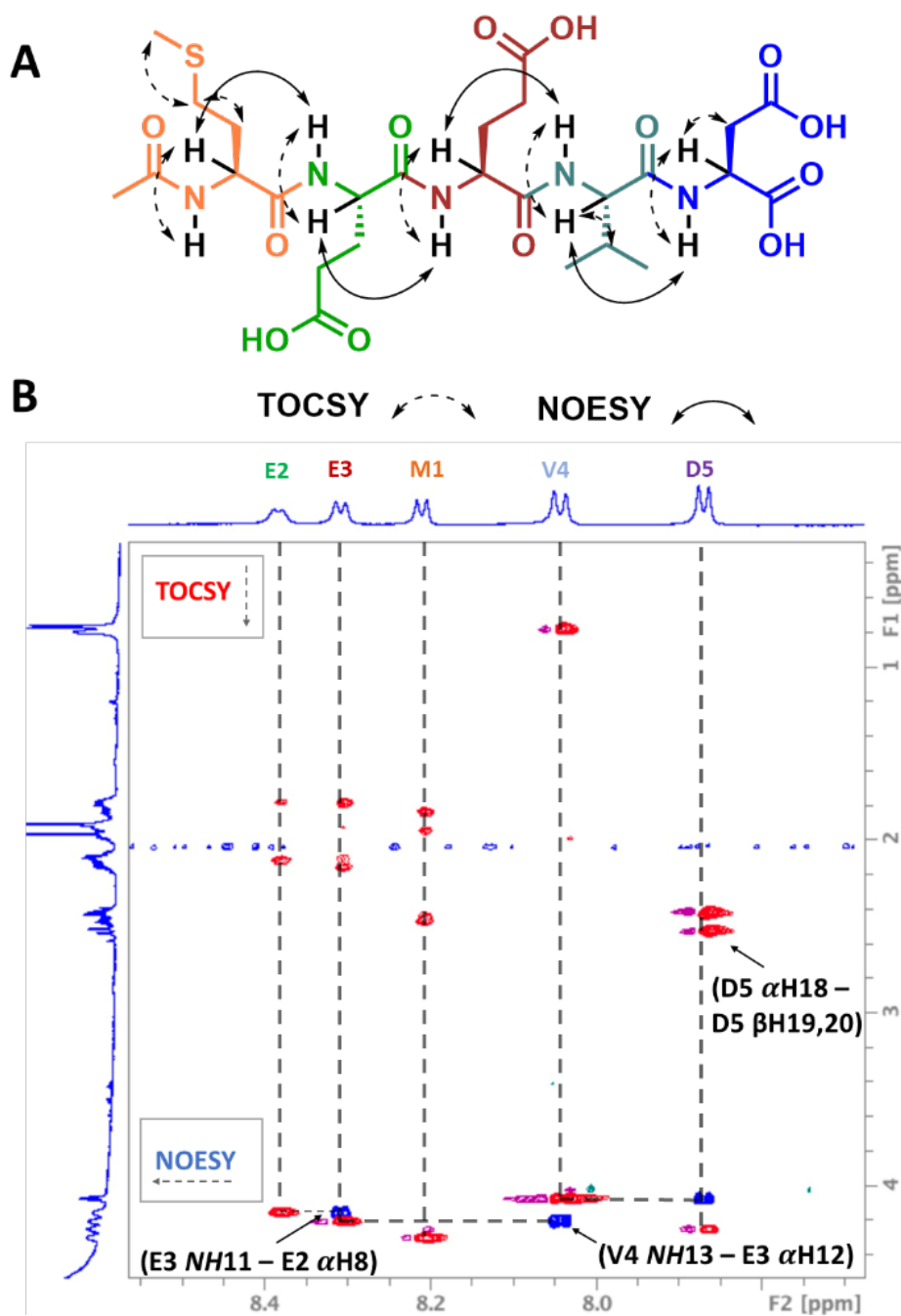
Figure 2. A: Representation of some key NOESY and TOCSY correlations which allowed for the unambiguous of the majority of proton resonances. **B:** Expanded and overlaid 2D TOCSY and NOESY spectra of peptide **1** (2mM), whilst bound to Hop$_{TPR2A}$ (40 µM) recorded in buffer with 10% D$_2$O at 298 K. TOCSY correlations read vertically, indicate key intra-residue correlations. NOESY correlations, read horizontally show correlations between α and *NH* protons from adjacent amino acid residues.

Reference ¹H spectrum
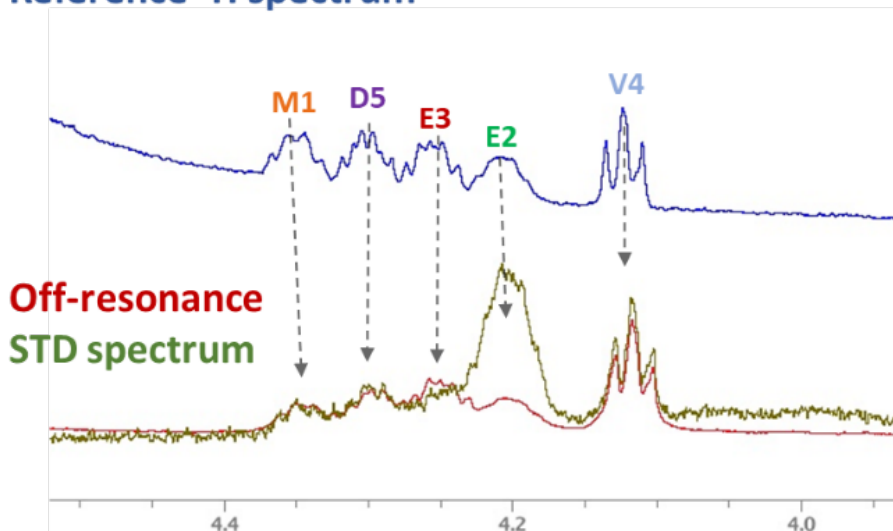
Figure 3. Stacked 1D ¹H expansions of Hop$_{TPR2A}$ – **1** complex. The reference ¹H spectrum is shown in blue, while the off-resonance and STD spectra are shown in red and green, respectively. The STD amplification factor for each unique signal was calculated as the percentage of signal in the off-resonance spectra over the signal intensity in the STD spectrum.
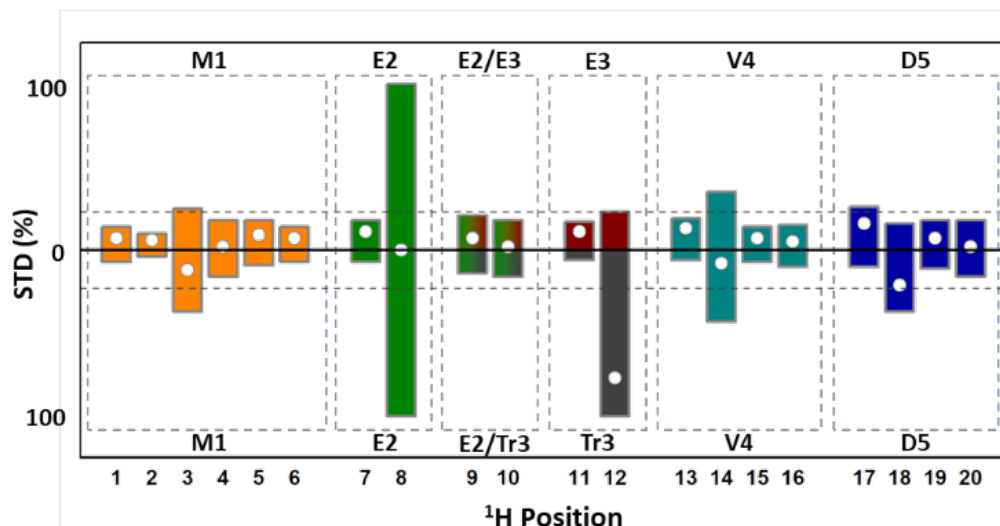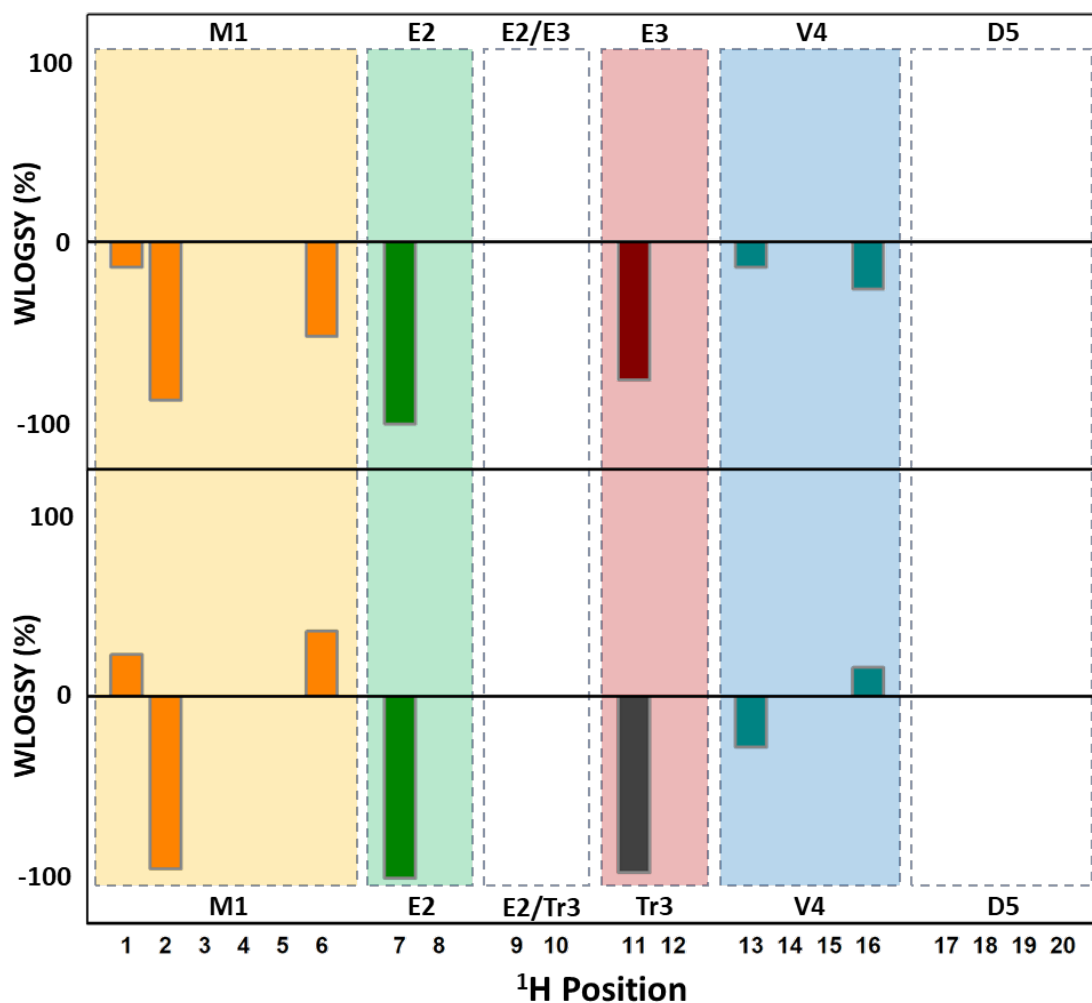
Figure 4. Comparative analysis of STD NMR data of the Hop_{TPR2A} – **1** (phased up) and Hop_{TPR2A} – **2** (phased down) complexes, respectively. Each residue is boxed off and shown in a different colour for clarity. The ambiguously assigned H-9 and H-10 are grouped together. ^1H Position correlates to numbering in **Figure 1B**. The horizontal dashed line depicts the mean STD intensity for each experiment. The height of each bar corresponds to the relative magnitude of the STD signal, whereas the white circles indicate the difference in magnitude between each experiment. In both complexes, the E2 α-proton (H-8) was the most prominent signal, indicating a central role in binding for both peptides. The most noticeable change was observed between the H-12 protons of each peptide, suggesting that the Tr3 α-proton makes a significant new interaction with Hop_{TPR2A}. In addition, the changes observed between H-17 and H-18 for peptides **1** and **2**, suggest a change in conformation in this region.
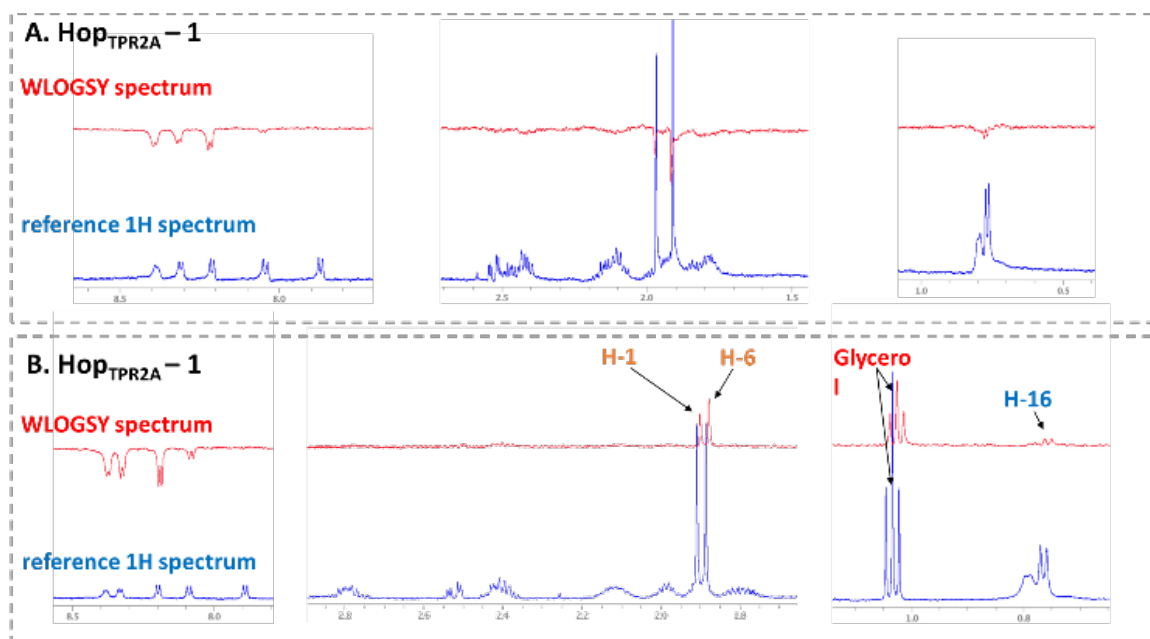
Figure 5. Stacked 1D ^{1}H expansions of the Hop_{TPR2A} – **1** (**A**) and Hop_{TPR2A} – **2** (**B**) complexes. The reference ^{1}H spectra are shown in blue and WLOGSY spectra are shown in red. The most noticeable change between the experiments are the un-inverted signals in panel B, corresponding to H-1 and H-6 respectively.

Figure 6. Comparative analysis of WLOGSY NMR data of the Hop$_{TPR2A}$ – **1** (top) and Hop$_{TPR2A}$ – **2** (bottom) complexes respectively. Figure formatting matches **Figure 4**. Regions where WLOGSY signals were detected are highlighted in colour. In both complexes, the E2 *NH* proton (H-7) was the most prominent signal, again like the STD data indicating a central role for E2 in binding for both peptides. The changes in WLOGSY signals, particularly the presence of +ve signals for H-1, H-6 and H-16, indicate substantial changes in the interaction of M1 and V4 with binding site waters for peptide **2** when compared to peptide **1**.
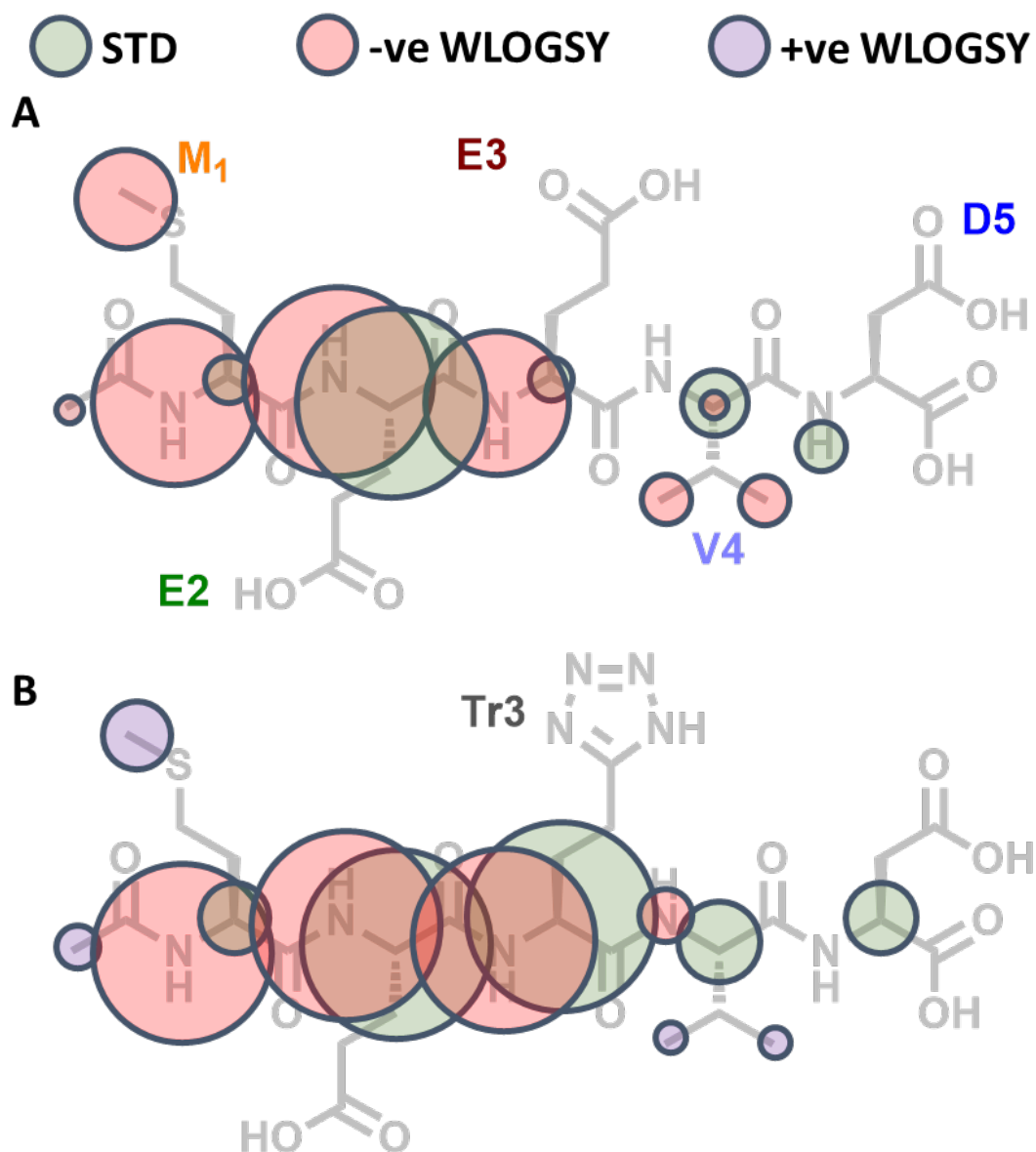
Figure 7. Summay of SliM observed NMR 'fingerprinting' of the Hop$_{TPR2A}$ – 1 (top) and Hop$_{TPR2A}$ – 2 (bottom) complexes, respectively. The bubble colour represents the mechanism of NOE magnetization, while bubble diameter is proportional to signal intensity. STD signals below the experimental mean and WLOGSY signals, which were supressed to 0% but not inverted were excluded. These data indicate differences in the interactions of both peptides with the target protein.
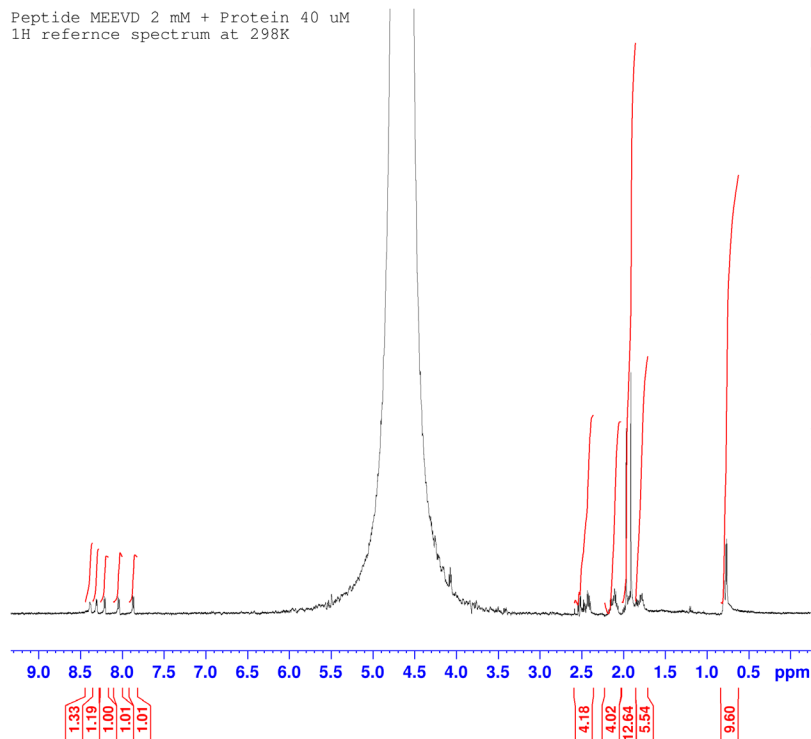
Supplementary Information

Table of Contents

1. Reference 1H NMR Spectra

Peptide MEEVD 2 mM + Protein 40 uM
1H refernce spectrum at 298K

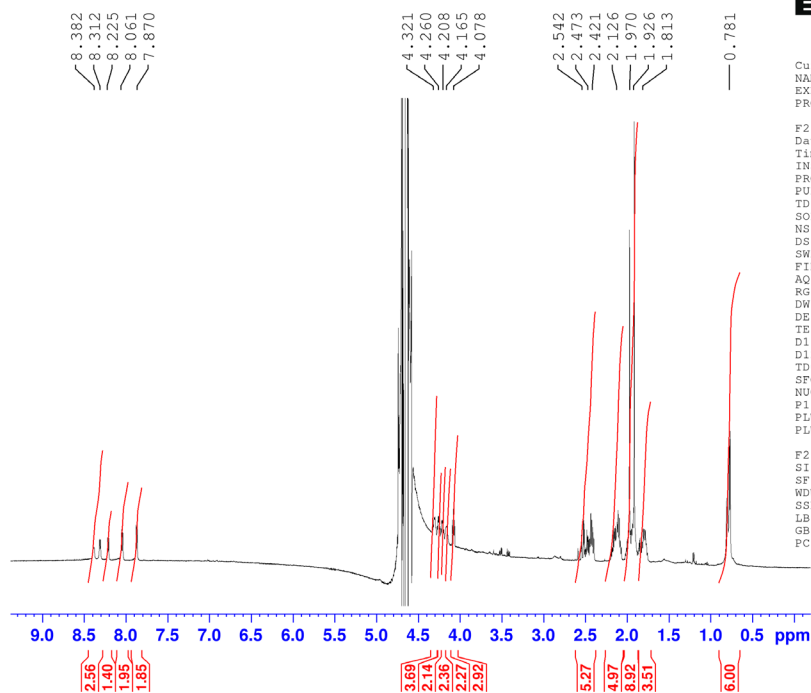Current Data Parameters
NAME   Daniel600
EXPNO   50
PROCNO   1

F2 - Acquisition Parameters
Date_   20231020
Time   15.32 h
INSTRUM   spect
PROBHD   Z130037_0007 (
PULPROG   zg30
TD   65536
SOLVENT   H2O+D2O
NS   64
DS   2
SWH   12019.230 Hz
FIDRES   0.366798 Hz
AQ   2.7262976 sec
RG   4.5
DW   41.600 usec
DE   18.00 usec
TE   298.0 K
D1   1.00000000 sec
TD0   1
SFO1   600.1037056 MHz
NUC1   1H
P0   3.97 usec
P1   11.90 usec
PLW1   28.00000000 W

F2 - Processing parameters
SI   65536
SF   600.1000262 MHz
WDW   EM
SSB   0
LB   0.30 Hz
GB   0
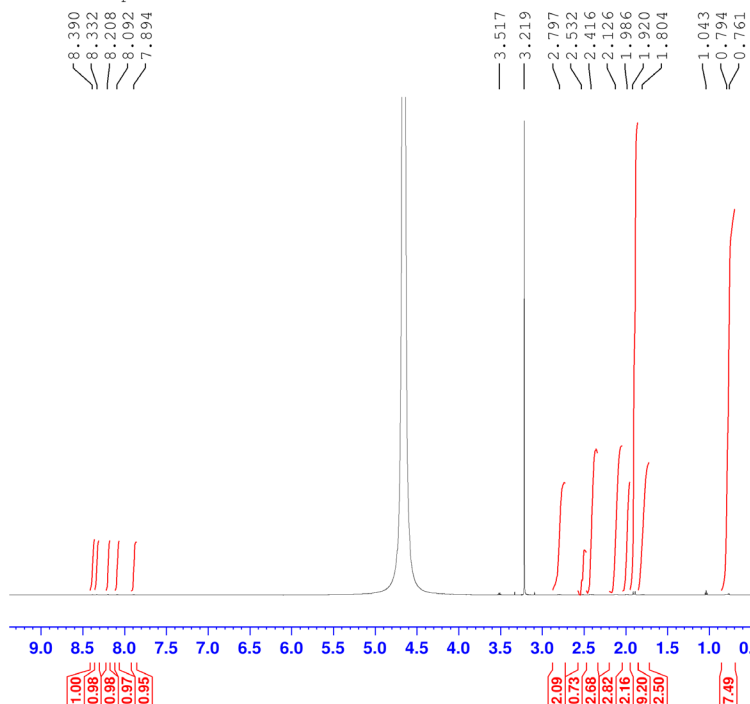PC   1.00

Peptide MEEVD 2 mM + Protein 40 uM
1H refernce spectrum at 298K

Current Data Parameters
NAME   Daniel600
EXPNO   51
PROCNO   1

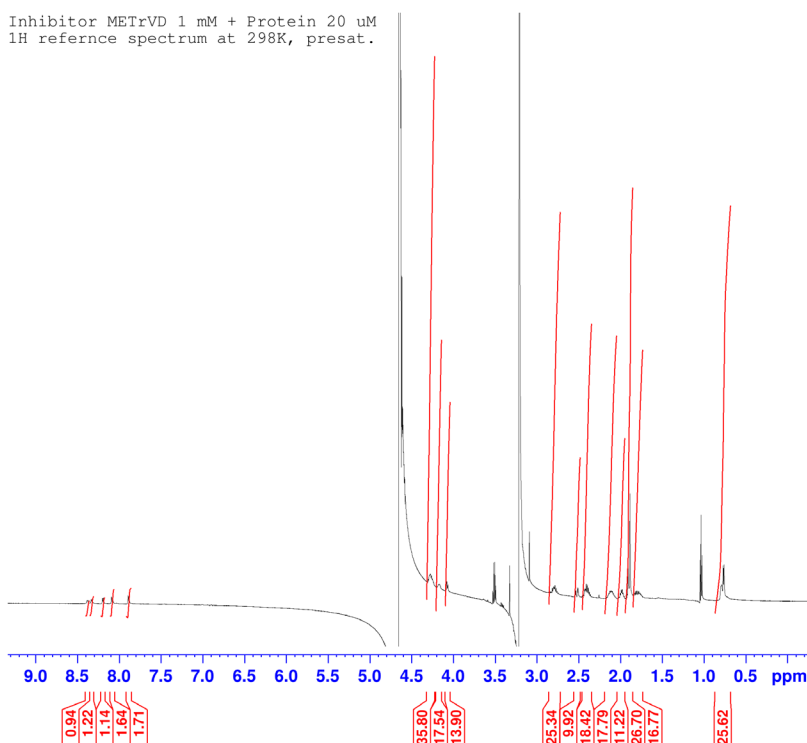F2 - Acquisition Parameters
Date_   20231020
Time   15.37 h
INSTRUM   spect
PROBHD   Z130037_0007 (
PULPROG   zgpr
TD   65536
SOLVENT   H2O+D2O
NS   64
DS   2
SWH   12019.230 Hz
FIDRES   0.366798 Hz
AQ   2.7262976 sec
RG   51.03
DW   41.600 usec
DE   18.00 usec
TE   298.0 K
D1   1.00000000 sec
D12   0.00002000 sec
TD0   1
SFO1   600.1028196 MHz
NUC1   1H
P1   11.90 usec
PLW1   28.00000000 W
PLW9   0.00015860 W

F2 - Processing parameters
SI   65536
SF   600.1000262 MHz
WDW   EM
SSB   0
LB   0.30 Hz
GB   0
PC   1.00

Inhibitor METrVD 1 mM + Protein 20 uM
1H refernce spectrum at 298K

8.390
8.332
8.208
8.092
7.894

3.517
3.219

2.797
2.532
2.416
2.126
1.986
1.920
1.804

1.043
0.794
0.761

1.00 0.98 0.98 0.97 0.95   2.09 0.73 2.68 2.82 2.16 9.20 2.50   7.49

Inhibitor METrVD 1 mM + Protein 20 uM
1H refernce spectrum at 298K, presat.

0.94 1.22 1.14 1.64 1.71   35.80 17.54 13.90   25.34 9.92 18.42 17.79 11.22 26.70 16.77   25.62

2. 2D NMR spectra for residue 1H assignments

2D TOCSY of MEEVD
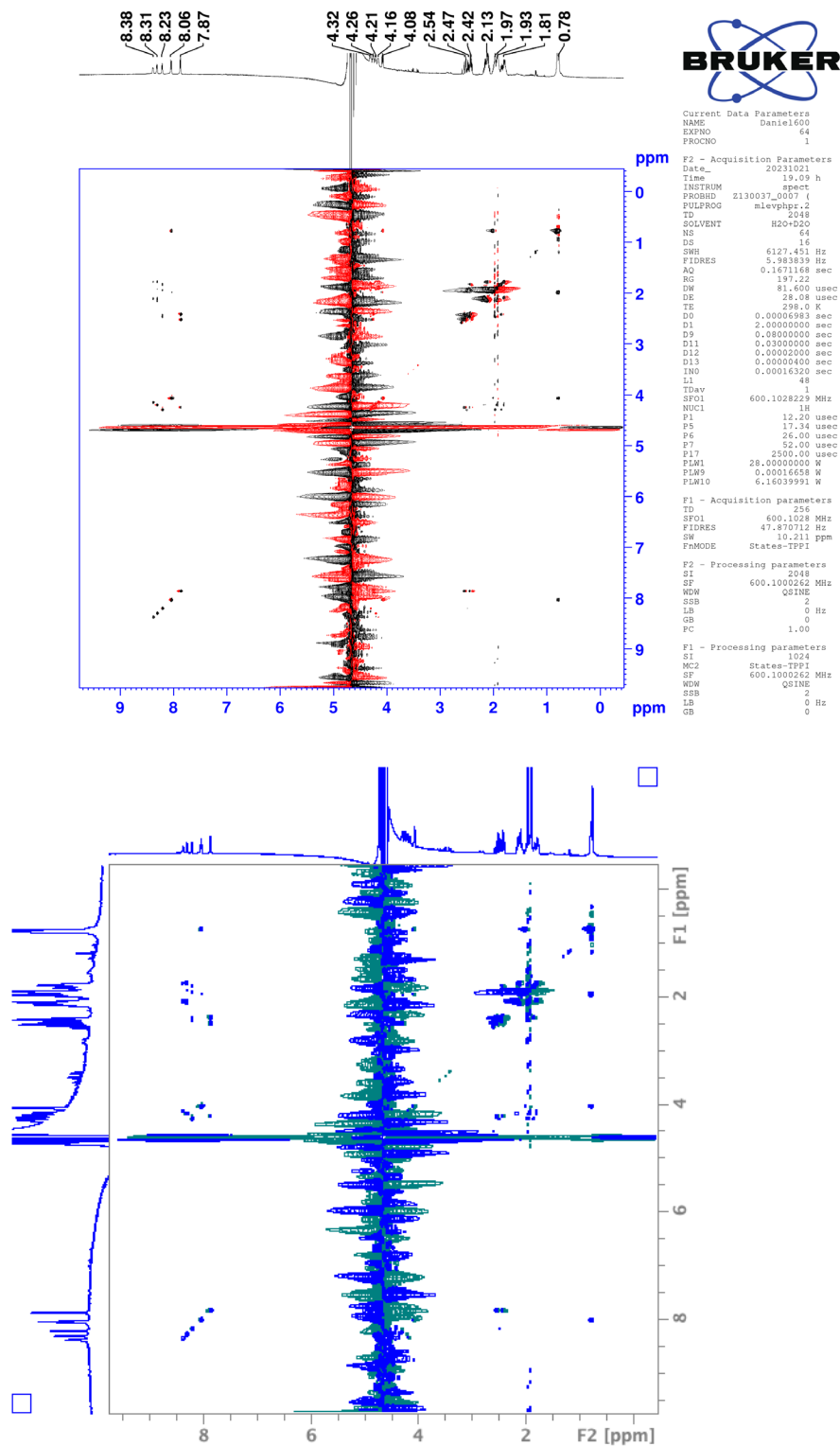
2D NOESY of MEEVD

MEEVD + P
2D NOESY spectrum at 298K
d8 0.8, ns 96

2D TOCSY of METrVD

3. Full 1H NMR Assignments

Table S1: Chemical Shifts of Peptides **1** and **2**, alongside STD and WLOGSY intensities

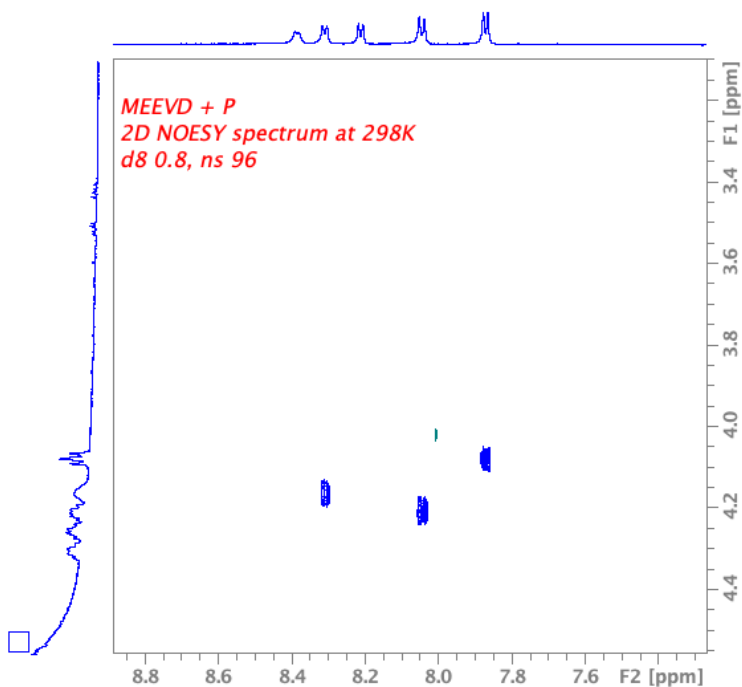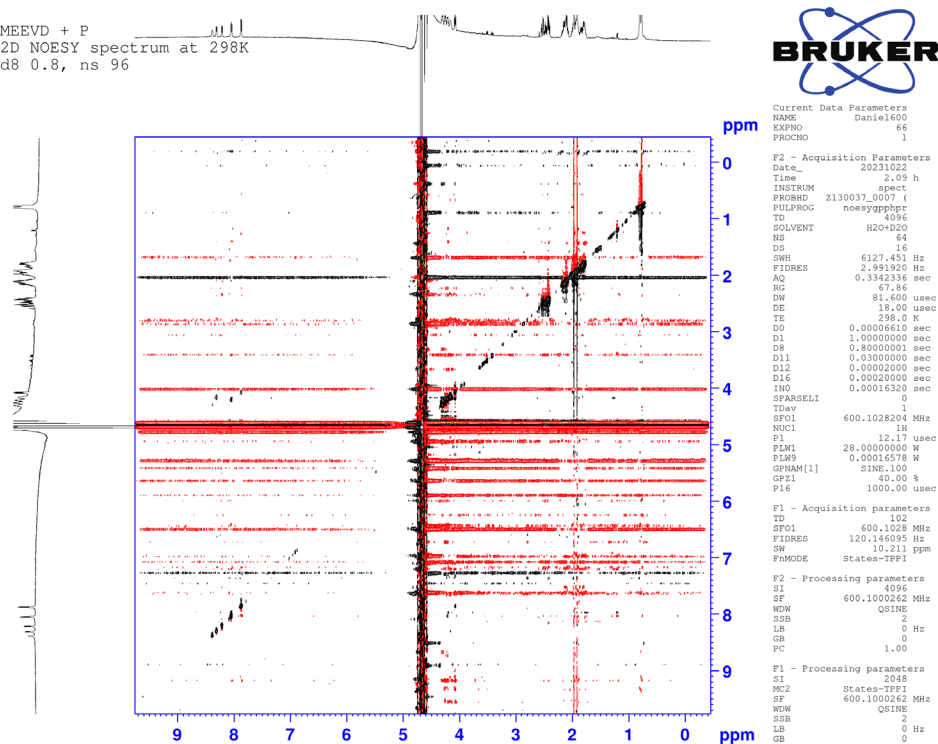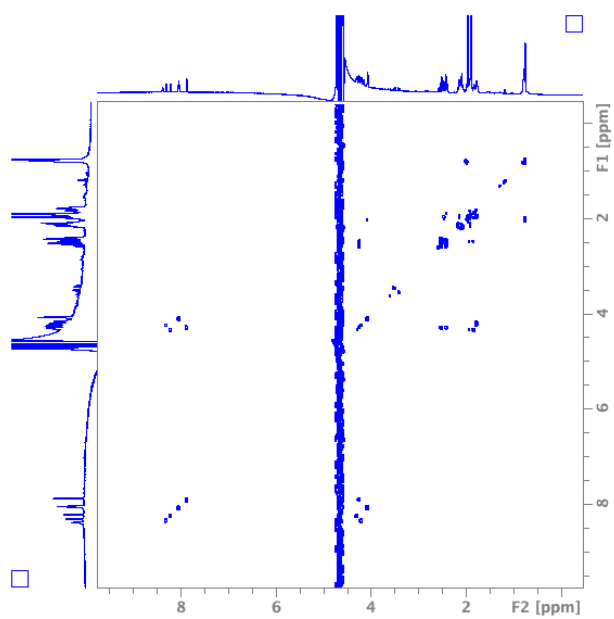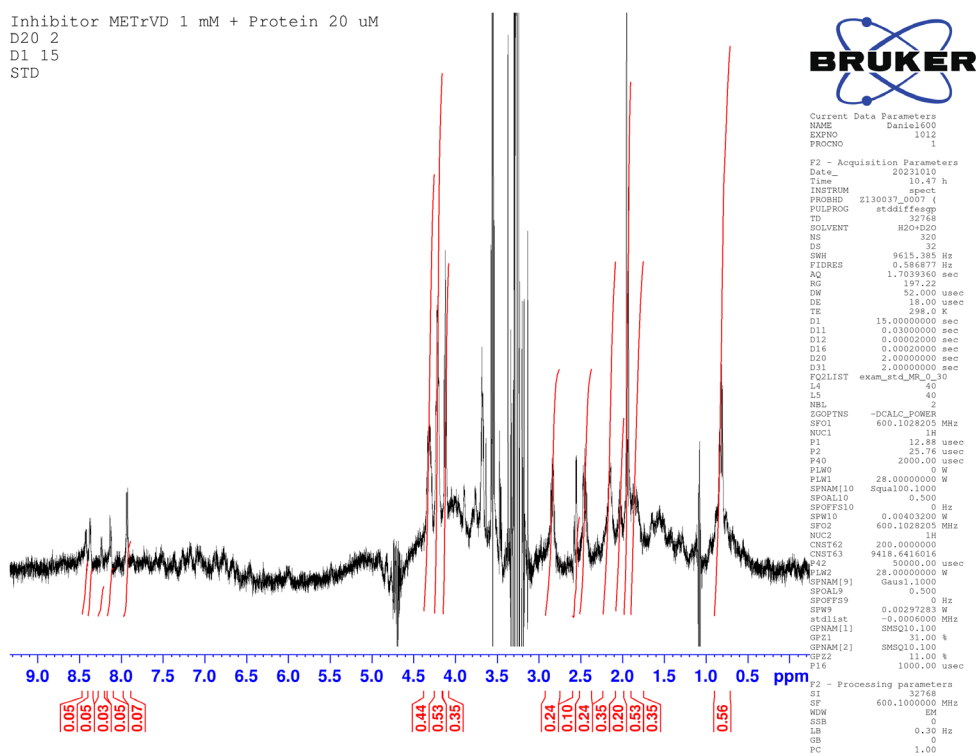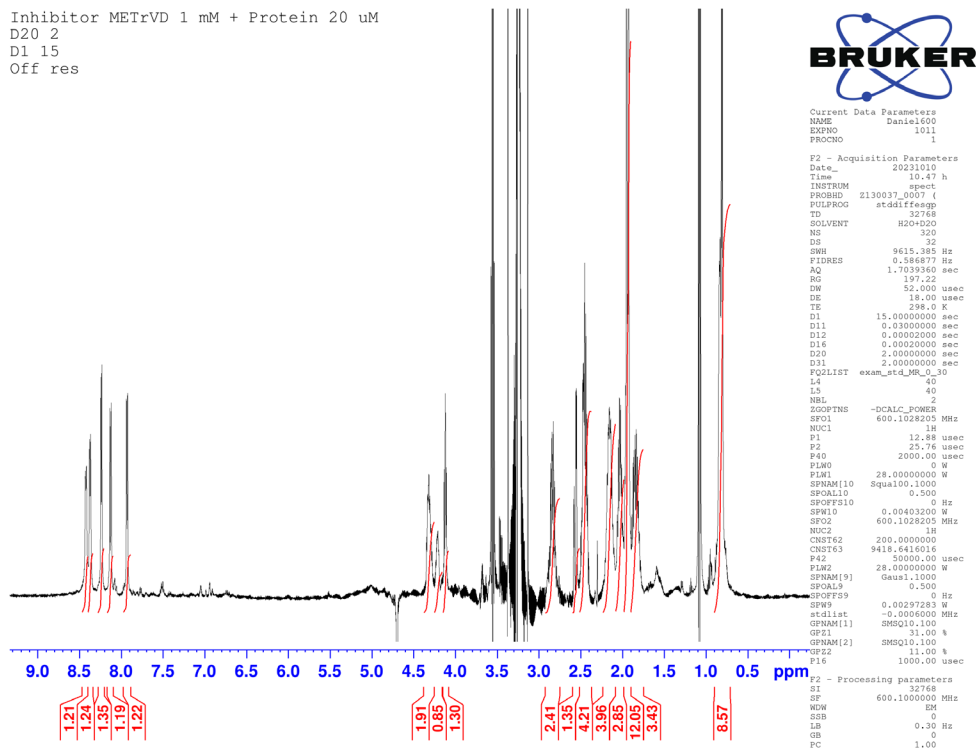|			MEEVD		
Proton Number	**Functional Group**	**Amino acid code**	**Chemical shift**	**STD %**	**WLOGSY %**
1	Ac	M1	1.98	14	-14
2	αNH	M1	8.21	10	-87
3	-CH	M1	4.33	25	0
4	R-CH2	M1	2.51	18	0
5	R-CH2	M1	1.88	18	0
6	SCH3	M1	1.90	14	-52
7	αNH	E2	8.4	18	-100
8	-CH	E2	4.21	100	0
9	R-CH2	E2, E3	2.14	21	0
10	R-CH2	E2, E3	1.81	18	0
11	αNH	E3	8.31	17	-76
12	-CH	E3	4.24	23	0
13	αNH	V4	8.05	19	-14
14	-CH	V4	4.11	35	0
15	R-CH(CH3)2	V4	1.99	14	0
16	R-CH(CH3)2	V4	0.78	15	-26
17	αNH	D5	7.87	26	0
18	-CH	D5	4.30	16	0
19	R-CH2	D5	2.45	18	0
20	R-CH2	D5	2.55	18	0
			Average	23	

			METrVD		
Proton Number	**Functional Group**	**Amino acid code**	**Chemical shift**	**STD %**	**WLOGSY %**
1	Ac	M1	2,01	7	23
2	αNH	M1	8,4	4	-95
3	-CH	M1	4,33	37	0
4	R-CH2	M1	2,51	16	0
5	R-CH2	M1	1,88	9	0
6	SCH3	M1	1,96	7	36
7	αNH	E2	8,36	7	-100
8	-CH	E2	4,21	100	0
9	R-CH2	E2, Tr3	2,14	14	0
10	R-CH2	E2, Tr3	1,81	16	0
11	αNH	Tr3	8,25	6	-97
12	-CH	Tr3	4,24	100	0
13	αNH	V4	8,12	6	-28
14	-CH	V4	4,12	43	0
15	R-CH(CH3)2	V4	1,99	7	0
16	R-CH(CH3)2	V4	0,78	10	16
17	αNH	D5	7,92	10	0
18	-CH	D5	4.30	37	0
19	R-CH2	D5	2,45	11	0
20	R-CH2	D5	2,55	16	0
			Average	23	

4. STD NMR Experiments

4.1 STD NMR spectra

Peptide MEEVD 2 mM + Protein 40 uM
D20 2
D1 15
Off res
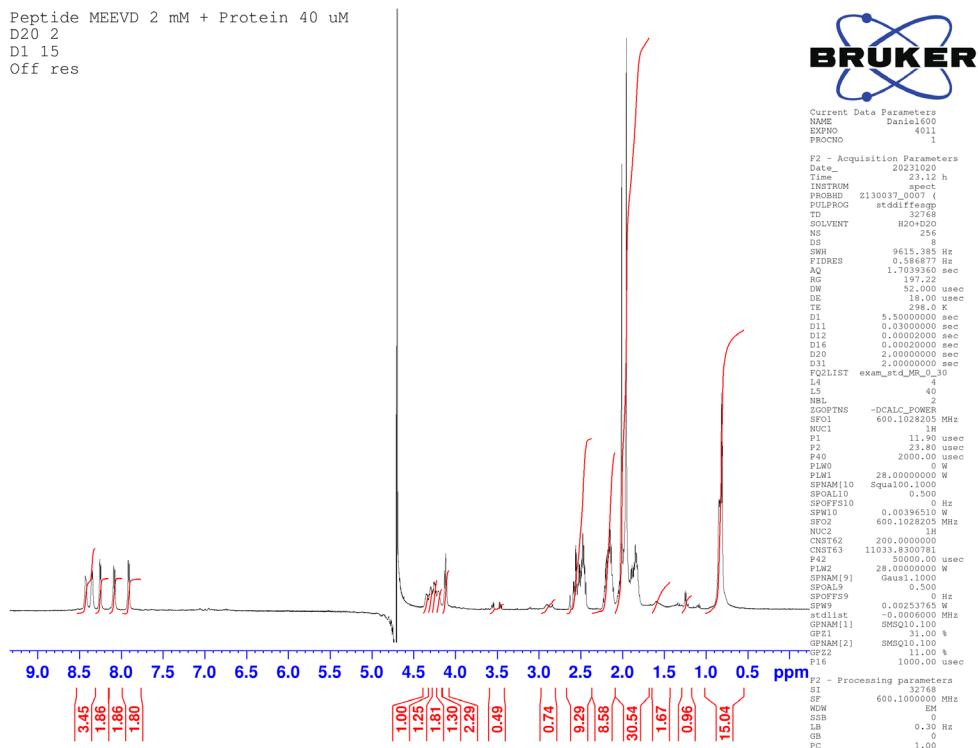
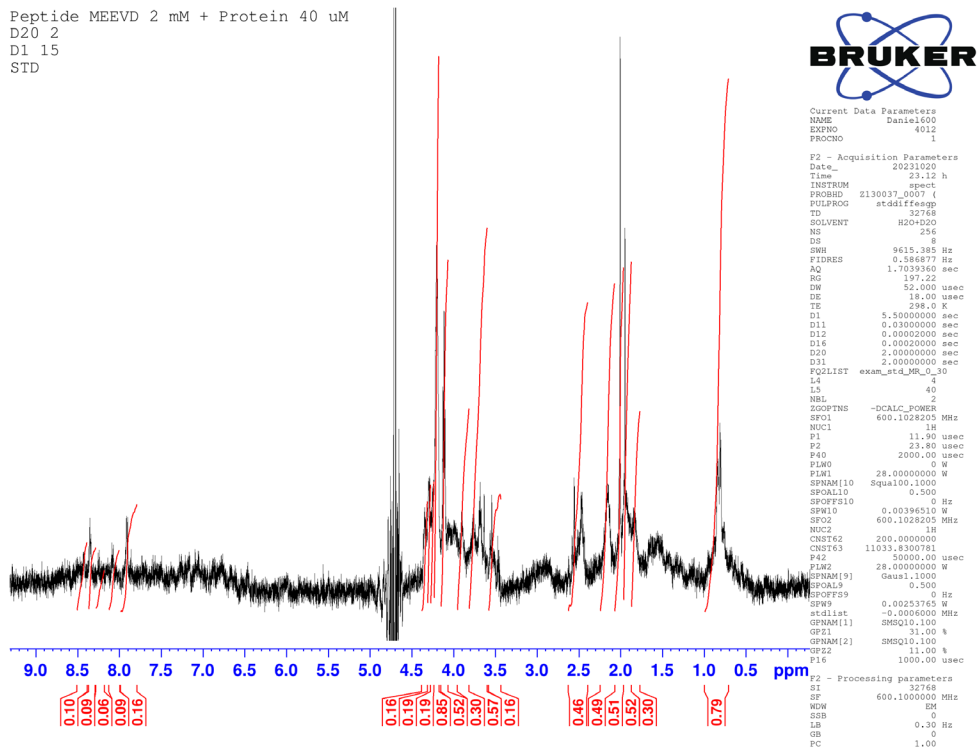Peptide MEEVD 2 mM + Protein 40 uM
D20 2
D1 15
STD

4.2 STD data

Table S2. STD Data determined for METrVD + Protein

STD Exp 1											
	S/N		Intensity (RI)		Signal region (ppm)	Noise region (ppm)	STD AMP (From RI)	STD% of MAX (From RI)	STD AMP (S/N)	STD% of MAX (From S/N)
METrVD	Off	STD DIFF	Off	STD DIFF						
NH	96,24	4,28	1,0793	0,0542	8,45-8,40	11,5-12,5	5,02	7,18	4,45	6,872705962
NH	119,94	5,58	1,064	0,0463	8,40-8,34	11,5-12,5	4,35	6,22	4,65	7,189683349
NH	171,33	3,5	1,2081	0,0304	8,30-8,20	11,5-12,5	2,52	3,60	2,04	3,156997504
NH	142,95	5,88	1,0651	0,0461	8,17-8,10	11,5-12,5	4,33	6,19	4,11	6,356715511
NH	150,3	8,98	1,0895	0,0741	7,98-7,90	11,5-12,5	6,80	9,72	5,97	9,233300396
α-CH	90,09	17,04	1,7074	0,4364	4,38-4,25	11,5-12,5	25,56	36,53	18,91	29,23025557
α-CH	47,49	30,73	0,764	0,5346	4,25-4,16	11,5-12,5	69,97	100,00	64,71	99,99999993
α-CH	149,82	35,73	1,1658	0,3525	4,15-4,07	11,5-12,5	30,24	43,21	23,85	36,85554456
R-CH/CH2/CH3	129,2	12,29	2,1555	0,242	2,93-2,73	11,5-12,5	11,23	16,04	9,51	14,70039411
R-CH/CH2/CH3	153,63	12,6	1,2057	0,0974	2,60-2,52	11,5-12,5	8,08	11,54	8,20	12,67459595
R-CH/CH2/CH3	246,95	13,42	3,7698	0,242	2,52-2,36	11,5-12,5	6,42	9,17	5,43	8,398139694
R-CH/CH2/CH3	140,02	11,79	3,5406	0,347	2,24-2,09	11,5-12,5	9,80	14,01	8,42	13,01257785
R-CH/CH2/CH3	146,75	9,71	2,5469	0,1993	2,09-1,98	11,5-12,5	7,83	11,18	6,62	10,22540996
R-CH/CH2/CH3	1796,72	90,97	10,7858	0,5333	1,98-1,90	11,5-12,5	4,94	7,07	5,06	7,824514534
R-CH/CH2/CH3	123,37	9,44	3,0683	0,3515	1,90-1,73	11,5-12,5	11,46	16,37	7,65	11,82502421
R-CH/CH2/CH3	608,97	22,85	7,6715	0,5623	0,92-0,70	11,5-12,5	7,33	10,47	3,75	5,798690311

Table S3. STD Data determined for MEEVD + Protein

STD Exp 1						
	Intensity (RI)		Signal region	Noise region	STD AMP (Fr	STD% of MA:
MEEVD	Off	STD DIFF				
E2	0,8691	0,0438	8,49-8,39	11,5-12,5	5,03969624	18,395019
E3	0,9813	0,0537	8,40-8,30	11,5-12,5	5,47233262	19,9741527
M1	0,9782	0,0273	8,30-8,20	11,5-12,5	2,79084032	10,1866379
V4	1,0035	0,0493	8,15-8,0	11,5-12,5	4,91280518	17,9318634
D5	0,9705	0,0717	7,96-7,86	11,5-12,5	7,38794436	26,9661841
α-CH	2,8806	0,7892	4,38-4,16	11,5-12,5	27,3970701	99,9999998
α-CH	1,2527	0,2722	4,16-4,08	11,5-12,5	21,7290652	79,3116386
D5 -CH2, M1	4,9609	0,2433	2,63-2,4	11,5-12,5	4,90435203	17,9010092
E2, E3 -CH2	4,5624	0,2622	2,26-2,08	11,5-12,5	5,74697528	20,9766054
M1 -CH3s, V:	11,7783	0,4678	2,08-1,92	11,5-12,5	3,97171069	14,4968446
E2, E3, M1 -(	4,441	0,2187	1,92-1,73	11,5-12,5	4,92456654	17,9747926
Val4 -CH3	7,5172	0,3087	0,92-0,70	11,5-12,5	4,10658224	14,9891292

Table S6. METrVD STD Buildup

STD AMP vs Saturation time D20 (s) (Using RI)							
D20	0	0,5	1	2	3	4	5
METrVD							
NH	0	2,6667848	5,600860292	5,02177337	6,299058085	5,946249649	5,134113743
NH	0	2,3981026	5,282167043	4,35150376	4,861174329	5,253875429	6,19710363
NH	0	1,65923725	4,445374634	2,51634798	3,030557421	3,258313739	3,347668437
NH	0	3,66578298	6,694363139	4,32823209	5,180905475	5,314941642	5,877184419
NH	0	5,14306411	9,727771068	6,80128499	7,798627002	7,480830372	8,28441583
α-CH	0	3,65508778	5,750692521	25,55933	25,24212706	25,25452324	23,0338683
α-CH	0	27,9049582	37,89256699	69,973822	69,07118644	65,09600808	62,12326239
α-CH	0	11,8392243	15,61365886	30,2367473	30,34042181	30,50717213	29,33981233
R-CH/CH2/CH3	0	8,97506166	6,181450837	11,2270935	13,86832709	9,456651488	8,775553214
R-CH/CH2/CH3	0	1,37296075	-0,987841945	8,07829477	9,173507611	6,758498469	6,670315921
R-CH/CH2/CH3	0	2,03991246	1,382858981	6,4194387	6,844950511	5,579197452	5,43623129
R-CH/CH2/CH3	0	2,71032999	3,099562585	9,80059877	9,793629306	8,940498296	8,887373875
R-CH/CH2/CH3	0	1,53232984	1,520622693	7,82519926	7,854428193	6,936393698	7,345177078
R-CH/CH2/CH3	0	1,51268116	2,609777844	4,94446402	5,420871335	5,583903677	5,715939647
R-CH/CH2/CH3	0	5,30488187	6,428316979	11,455855	12,24228075	10,44123241	9,154713743
R-CH/CH2/CH3	0	3,48770153	5,024871755	7,32972691	7,326638853	6,936536683	6,454108273